

Published in final edited form as:

Science. 2014 September 5; 345(6201): 1170–1173. doi:10.1126/science.1254237.

A complex iron-calcium cofactor catalyzing phosphotransfer chemistry

Shee Chien Yong^{#1}, Pietro Roversi^{#2,3}, James Lillington^{2,4}, Fernanda Rodriguez¹, Martin Krehenbrink^{1,5}, Oliver B. Zeldin^{1,6}, Elspeth F. Garman¹, Susan M. Lea^{2,*}, and Ben C. Berks^{1,*}

¹Department of Biochemistry, University of Oxford, South Parks Road, Oxford OX1 3QU, United Kingdom

²Sir William Dunn School of Pathology, University of Oxford, South Parks Road, Oxford OX1 3RE, United Kingdom

These authors contributed equally to this work.

Abstract

Alkaline phosphatases play a crucial role in phosphate acquisition by microorganisms. To expand our understanding of catalysis by this class of enzymes we have determined the structure of the widely-occurring microbial alkaline phosphatase PhoX. The enzyme contains a complex active site cofactor comprising two antiferromagnetically-coupled Fe³⁺ ions, three Ca²⁺ ions, and a μ₃-bridging oxo group. Notably, the main part of the cofactor resembles synthetic oxide-centered triangular metal complexes. Structures of PhoX-ligand complexes reveal how the active site metal ions bind substrate and implicate the cofactor oxo group in the catalytic mechanism. The presence of iron in PhoX raises the possibility that iron bioavailability limits microbial phosphate acquisition.

Phosphate-containing macromolecules and metabolites are essential components of living cells. Under conditions of phosphate deficiency microorganisms obtain phosphate from biologically-derived organic compounds by producing extra-cytoplasmic alkaline phosphatases (1, 2). Prominent amongst these enzymes are phosphate monoesterases of the PhoA and PhoX families which are found in all three domains of life. The archetypal PhoA enzyme of *Escherichia coli* has been extensively studied (2) but PhoX alkaline phosphatases are minimally characterized and do not exhibit sequence similarity to other phosphotransfer enzymes. Genes encoding PhoX are abundant in ocean bacteria (3-5) and are also present in bloom-forming cyanobacteria (6), human pathogens (7, 8), and eukaryotic green algae including the model organism *Chlamydomonas reinhardtii* (9).

*Correspondence to: ben.berks@bioch.ox.ac.uk (BCB); susan.lea@path.ox.ac.uk (SML).

³Current address: Department of Biochemistry, University of Oxford, South Parks Road, Oxford OX1 3QU, United Kingdom.

⁴Current address: Department of Biological Sciences, Birkbeck College, Malet Street, London WC1E 7HX, United Kingdom.

⁵Current address: Cysal GmbH, Mendelstrasse 11, 48149 Münster, Germany.

⁶Current address: Stanford University, School of Medicine, James H. Clark Center, 318 Campus Drive, Stanford, CA 94305-5432, United States of America.

To establish the active site architecture of PhoX we have undertaken structural analysis of the enzyme from *Pseudomonas fluorescens* Pf0-1 (10). Recombinant *P. fluorescens* PhoX is a phosphomonoesterase with no phosphodiesterase activity and is able to cleave phosphorus-nitrogen bonds but not phosphorus-carbon bonds (Fig. S1A). The purified PhoX protein is purple in color with several broad absorbance bands in the visible spectrum, indicating the presence of a prosthetic group (Fig. 1A). Addition of the non-hydrolysable substrate analogue adenosine-5'-(β,γ -methylene)triphosphate (AMP-PCP) causes changes in the visible spectrum (Fig. 1A) showing that the prosthetic group is associated with the substrate-binding site. We determined crystal structures for native PhoX and for PhoX in complex with AMP-PCP, phosphate, and the putative transition state mimic vanadate. All four structures were determined to high resolution (1.1-1.5 Å) from crystals grown at the catalytic pH optimum of 8 (Figs. S1B, S2A, S3, Tables S1, S2).

PhoX folds as a 6-bladed β -propeller (Fig. 2A). The active site of the enzyme lies at the bottom of the cavity at the center of the propeller and is accessible from only one face of the propeller through a channel (Fig. 2B). The active site in the native PhoX structure contains four metal ions, and a further metal ion is present in the structures of the three PhoX-ligand complexes. Proton-induced X-ray emission spectroscopy of a sample of the PhoX-phosphate complex detected 3.4 ± 0.3 atoms of calcium and 1.6 ± 0.1 atoms of iron per complex with no other candidate elements (Co, Ni, Zn, Mg, Mn) detectable. Individual metal ion sites in the PhoX structures were assigned as three Ca and two Fe ions on the basis of their coordination geometry and anomalous scattering at different wavelengths (Fig. S2B,C). All metal sites are fully occupied and the B factors for the Ca ions do not differ significantly from those for the Fe ions. The ions Fe_A , Fe_B , and Ca_A form a triangle at the bottom of the active site cavity (Figs. 2 and 3). Ions Ca_B and (in the ligand complexes only) Ca_C lie above the plane of the first three ions and to one side of the cavity, with the plane containing the three Ca ions being almost perpendicular to that of the $Fe_A Fe_B Ca_A$ triangle. All five metal ions are co-ordinated by oxygen atoms provided either by the side chains of conserved residues, by water, or by the ligand molecules (Figs. 2C, S3, S4A,D,E, Table S3). Fe_A is additionally ligated by a thiolate side chain from invariant Cys179. Substitution of individual amino acids co-ordinating Fe_A , Fe_B , Ca_B , or Ca_C resulted in PhoX variants with either no, or trace, catalytic activity (Table S4).

Electron paramagnetic resonance (EPR) spectroscopy was used to determine the oxidation state of the PhoX iron atoms (Fig. 1B). The native PhoX protein was EPR silent. However, partial reduction of the protein with dithionite led to the appearance of a $g=4.3$ EPR signal characteristic of monomeric high spin Fe^{3+} . This behavior suggests that PhoX contains a pair of high spin Fe^{3+} ions rendered EPR-silent by magnetic coupling, with reduction of one of the Fe^{3+} ions to the EPR-silent Fe^{2+} state revealing the EPR signal from the remaining Fe^{3+} ion. Because the two ions in the resulting mixed valence state no longer interact magnetically it can be inferred that the Fe^{2+} ion has been released from the active site cofactor. Thus, only the fully oxidized Fe^{3+} - Fe^{3+} state of the PhoX cofactor is catalytically viable. Further addition of sodium dithionite led to reduction of the remaining Fe^{3+} ion, rendering PhoX EPR silent again.

Within the $\text{Fe}_A\text{Fe}_B\text{Ca}_A$ triangle lies an atom that is within bonding distance of all three metal ions (Fig. 2C; Table S3). The close to in-plane geometry suggests that this atom is an oxide ion (O^{2-}). This is confirmed by the structural identity between this part of the PhoX active site and $\text{Fe}_2\text{CaO}(\text{CCl}_3\text{COO})_6(\text{THF})_4$, an inorganic complex containing a μ_3 -oxo-bridged $\text{Fe}^{3+}\text{Fe}^{3+}\text{Ca}^{2+}$ cluster with O-donor co-ordination (11)(Fig. S5). The presence of a bridging oxo group explains the strong antiferromagnetic coupling of the two Fe^{3+} ions observed by EPR spectroscopy (Fig. 1B). The intense visible absorption bands observed for PhoX (Fig. 1A) are, likewise, characteristic of an oxo-bridged dinuclear Fe^{3+} unit (12), although Cys179 thiolate-to- Fe_A^{3+} ligand-to-metal charge transfer bands are also expected to contribute to the visible spectrum (13). The purple color of PhoX is, thus, distinct in origin from that of the well-known purple acid phosphatases in which the visible absorption is due to a tyrosinate-to- Fe^{3+} charge transfer (14).

PhoX had previously been considered to be an exclusively Ca-dependent enzyme based on the results of metal ion reconstitution experiments (e.g (7, 8, 15)) (although a biosynthetic requirement for Fe in *P. fluorescens* PhoX biosynthesis had been reported (16)). In agreement with these earlier reconstitution studies, we found that the enzymatic activity of *P. fluorescens* PhoX was abolished by the metal ion chelator EDTA and that activity could be restored by the addition of Ca^{2+} ions alone (Fig. S1C). However, EDTA treatment perturbed, rather than abolished, the visible transitions arising from the $\text{Fe}_A\text{-Fe}_B$ pair, indicating that the Fe^{3+} ions remain bound to PhoX in the presence of EDTA (Fig. 1C). This conclusion was confirmed by EPR spectroscopy, which showed that only a small proportion (12% by spin quantitation) of the Fe bound to PhoX is extracted by 50mM EDTA (Fig. 1B). Addition of Ca^{2+} ions to EDTA-treated enzyme restored the visible spectrum (Fig. 1C).

The PhoX-ligand complex structures show that the active site metal ions form a scaffold that binds the terminal phosphoryl group of the substrate molecule. In the phosphate and vanadate complexes all five metal ions have bonding interactions with the three terminal oxygen atoms of the ligand (Figs. 2C, 3C, S4B,C). In these structures the ligand sits on the $\text{Fe}_A\text{Fe}_B\text{Ca}_A$ unit, with each terminal oxygen atom of the ligand placed above one of the three metal ions. In the AMP-PCP-bound structure the phosphate group has a tilted orientation relative to the $\text{Fe}_A\text{Fe}_B\text{Ca}_A$ plane and there is no interaction with Ca_A (Fig. 3B). This binding mode permits both the terminal and β -phosphate groups of AMP-PCP to make bonding interactions with Ca_A and Ca_B (Fig. 3B). Modeling studies (not shown) suggest that even for substrates without multiple phosphate groups an initial tilted binding mode will usually be favored in order to avoid steric clashes with Ca_A and Ca_B . The sole conformational change in the protein that takes place on ligand binding to PhoX is movement of the guanidinium head group of conserved Arg385 to form a bonding interaction with one of the terminal oxygen atoms of the ligand (Fig. 2C). Replacing this arginine residue with alanine impairs PhoX activity suggesting Arg385 contributes to catalysis (Table S4).

The primary mechanism of rate enhancement by phosphoryl transfer enzymes is thought to be provision of favorable geometric and electrostatic interactions with the transition state (1, 2). PhoX provides high valency metal ions that are appropriately positioned to interact with all three terminal oxygen atoms of the phosphoryl group, and in the vanadate complex the

ligand is significantly distorted towards the presumed transition state geometry (Fig. S4C). Leaving group activation through co-ordination of the oxygen atom of the labile bond by Ca_C may also contribute to catalysis (Figs. 3C,E, S4B)(2).

Enzymatic phosphoryl transfer reactions involve in-line displacement of the leaving group by a nucleophile (2). Examination of the PhoX-ligand structures shows that the metal-bridging oxide ion is the only plausible candidate nucleophile (Figs. 3B-C, S4B,C). In the phosphate and vanadate complexes the oxide ion is positioned below the phosphorus atom and is directly in line with the scissile bond. It also blocks access of other potential nucleophiles to the substrate phosphorus atom *trans* to the leaving group in all three PhoX-ligand complexes (the calculated water-accessible surface area of the phosphorus atom in each case is 0.0 \AA^2). There is small molecule precedent for the hydrolysis of phosphate esters by an oxide ion bridging two Co^{3+} ions (17) and a metal-bridging oxide nucleophile has also been inferred to be present in one purple acid phosphatase (18). Oxide movement towards the phosphoryl P atom during catalysis would be facilitated by the weak Ca_A -oxide interaction and would be consistent with the observed movement of the oxide relative to the $\text{Fe}_A\text{Fe}_B\text{Ca}_A$ plane in response to ligand binding at the active site ($+0.4/-0.2 \text{ \AA}$; Figs. 3A-C, S4B). Due to the difficulty in abstracting a μ -bridging oxygen atom from between two Fe^{3+} ions it is likely that the initial reaction product is resolved by a second in-line nucleophilic attack by a water molecule from the opposite side of the phosphorus atom (Fig. 3D). This water molecule would plausibly be activated by binding to Ca_C since this ion already interacts at the equivalent position with the oxygen atom of the substrate scissile bond (Figs. 3C,D, S4B). Nevertheless, we cannot exclude the possibility that the active site environment labilizes the μ -bridging oxygen atom to allow release of the initial product.

Our structural analysis suggests that PhoX has an almost exclusively inorganic mechanism in which the protein serves as a matrix for the catalytic metal ions. Unique features of the PhoX active site include a cofactor that combines Fe and Ca ions, Cys co-ordination to a Fe^{3+} ion that lacks a redox function, and the use of more than three metal ions to interact with a single phosphoryl group. It is also notable that the $\text{Fe}_A\text{Fe}_B\text{Ca}_A\text{O}$ fragment of the cofactor resembles extensively-studied synthetic oxide-centered triangular metal complexes (19). Carboxylate-bridged Fe^{3+} pairs are used in other enzymes to catalyze redox reactions with oxygen (12) but in PhoX perform a non-redox role in which the high charge of the iron atoms is exploited to polarize the substrate. Like PhoX, some purple acid phosphatases use a di-iron center to carry out phosphoryl transfer reactions (20). However, in contrast to PhoX, the enzymatically active oxidation state of the iron pair is $\text{Fe}^{3+}\text{-Fe}^{2+}$ (21) and the catalytic nucleophile is probably a metal-bridging hydroxide ion (20).

Genes coding for PhoX and PhoA are not normally found in the same bacterium (4) suggesting that these two types of alkaline phosphatase have equivalent physiological roles. PhoA activity depends on Zn^{2+} ions, which are present at low abundance in many environments (22), and this has led to the hypothesis that organisms expressing PhoX have an advantage in P and Zn co-limited environments (15). However, our observation that PhoX requires Fe^{3+} ions as cofactors implies that PhoX activity will also be metal-limited by the low bioavailability of Fe in many environments (23). This hypothesis challenges the assumption that P and Fe have biochemically independent effects in co-limiting conditions

(24) and raises the possibility that combined Zn-Fe-P co-limitation may occur in some environments through the requirement for either Zn or Fe for phosphate acquisition from organic phosphates. An environment where such considerations may apply is the Western North Atlantic where inorganic P and Zn concentrations are very low and Fe can also be in short supply (22, 25, 26).

Supplementary Material

Refer to Web version on PubMed Central for supplementary material.

Acknowledgments

We thank G. O'Toole for providing *P. fluorescens* Pf0-1 genomic DNA, J. Marcoux, B. Pilgrim, and A. Parkin for exploratory experiments, and F. Armstrong, T. Browning, J. McGrady, G. Henderson, D. Herschlag, C. Schofield, A. Thomson, C. Timmel, N. Williams, and R. Williams for valuable discussions. This work was funded by the University of Oxford, Pembroke College Oxford, Oxford Martin School Vaccine Design Institute, the Engineering and Physical Sciences Research Council, the Biotechnology and Biological Sciences Research Council (grant F02150X), and the European Molecular Biology Organization. Structure co-ordinates and X-ray data have been deposited in the PDB with accession codes 4a9v, 4amf, 4alf, and 3zwu.

References and Notes

1. Kamerlin SC, Sharma PK, Prasad RB, Warshel A. Why nature really chose phosphate. Quarterly reviews of biophysics. 2013; 46:1–132. [PubMed: 23318152]
2. Lassila JK, Zalatan JG, Herschlag D. Biological phosphoryl-transfer reactions: understanding mechanism and catalysis. Annual review of biochemistry. 2011; 80:669–702.
3. Luo H, Benner R, Long RA, Hu J. Subcellular localization of marine bacterial alkaline phosphatases. Proceedings of the National Academy of Sciences of the United States of America. 2009; 106:21219–21223. [PubMed: 19926862]
4. Sebastian M, Ammerman JW. The alkaline phosphatase PhoX is more widely distributed in marine bacteria than the classical PhoA. The ISME journal. 2009; 3:563–572. [PubMed: 19212430]
5. Orchard ED, Webb EA, Dyhrman ST. Molecular analysis of the phosphorus starvation response in *Trichodesmium* spp. Environmental microbiology. 2009; 11:2400–2411. [PubMed: 19555381]
6. Harke MJ, Berry DL, Ammerman JW, Gobler CJ. Molecular response of the bloom-forming cyanobacterium, *Microcystis aeruginosa*, to phosphorus limitation. Microbial ecology. 2012; 63:188–198. [PubMed: 21720829]
7. van Mourik A, Bleumink-Pluym NM, van Dijk L, van Putten JP, Wosten MM. Functional analysis of a *Campylobacter jejuni* alkaline phosphatase secreted via the Tat export machinery. Microbiology. 2008; 154:584–592. [PubMed: 18227262]
8. Roy NK, Ghosh RK, Das J. Monomeric alkaline phosphatase of *Vibrio cholerae*. Journal of bacteriology. 1982; 150:1033–1039. [PubMed: 6804434]
9. Moseley JL, Chang CW, Grossman AR. Genome-based approaches to understanding phosphorus deprivation responses and PSR1 control in *Chlamydomonas reinhardtii*. Eukaryotic cell. 2006; 5:26–44. [PubMed: 16400166]
10. Materials and methods are available on *Science* online.
11. Prodius D, et al. Synthesis, structure and properties of heterotrinnuclear carboxylate complexes $[\text{Fe}_2\text{M}(\text{Ca}, \text{Sr}, \text{Ba})\text{O}(\text{CCl}_3\text{COO})_6(\text{THF})_n]$. Polyhedron. 2006; 25:2175–2182.
12. Solomon EI, et al. Geometric and electronic structure/function correlations in non-heme iron enzymes. Chemical reviews. 2000; 100:235–349. [PubMed: 11749238]
13. Oganessian VS, Thomson AJ. Magnetic circular dichroism of symmetry and spin forbidden transitions of high-spin metal ions. J Chem Phys. 2000; 113:5003–5017.

14. Gaber BP, Sheridan JP, Bazer FW, Roberts RM. Resonance Raman scattering from uteroferrin, the purple glycoprotein of the porcine uterus. *The Journal of biological chemistry*. 1979; 254:8340–8342. [PubMed: 468828]
15. Kathuria S, Martiny AC. Prevalence of a calcium-based alkaline phosphatase associated with the marine cyanobacterium *Prochlorococcus* and other ocean bacteria. *Environmental microbiology*. 2011; 13:74–83. [PubMed: 20649645]
16. Monds RD, Newell PD, Schwartzman JA, O'Toole GA. Conservation of the Pho regulon in *Pseudomonas fluorescens* Pf0-1. *Applied and environmental microbiology*. 2006; 72:1910–1924. [PubMed: 16517638]
17. Williams NH, Lebus AM, Chin J. A structural and functional model of dinuclear metallophosphatases. *Journal of the American Chemical Society*. 1999; 121:3341–3348.
18. Schenk G, et al. Phosphate forms an unusual tripodal complex with the Fe-Mn center of sweet potato purple acid phosphatase. *Proceedings of the National Academy of Sciences of the United States of America*. 2005; 102:273–278. [PubMed: 15625111]
19. Cannon RD, White RP. Chemical and physical properties of triangular bridged metal complexes. *Prog Inorg Chem*. 1988; 36:195–298.
20. Mitic N, et al. The catalytic mechanisms of binuclear metallohydrolases. *Chemical reviews*. 2006; 106:3338–3363. [PubMed: 16895331]
21. Wang DL, Holz RC, David SS, Que L Jr, Stankovich MT. Electrochemical properties of the diiron core of uteroferrin and its anion complexes. *Biochemistry*. 1991; 30:8187–8194. [PubMed: 1868093]
22. Jakuba RW, Moffett JW, Dyhrman ST. Evidence for the linked biogeochemical cycling of zinc, cobalt, and phosphorus in the western North Atlantic Ocean. *Global Biogeochem Cy*. 2008; 22
23. Moore CM, et al. Processes and patterns of oceanic nutrient limitation. *Nat Geosci*. 2013; 6:701–710.
24. Saito MA, Goepfert TJ, Ritt JT. Some thoughts on the concept of colimitation: Three definitions and the importance of bioavailability. *Limnol Oceanogr*. 2008; 53:276–290.
25. Wu JF, Sunda W, Boyle EA, Karl DM. Phosphate depletion in the western North Atlantic Ocean. *Science*. 2000; 289:759–762. [PubMed: 10926534]
26. Moore CM, et al. Iron limits primary productivity during spring bloom development in the central North Atlantic. *Global Change Biol*. 2006; 12:626–634.

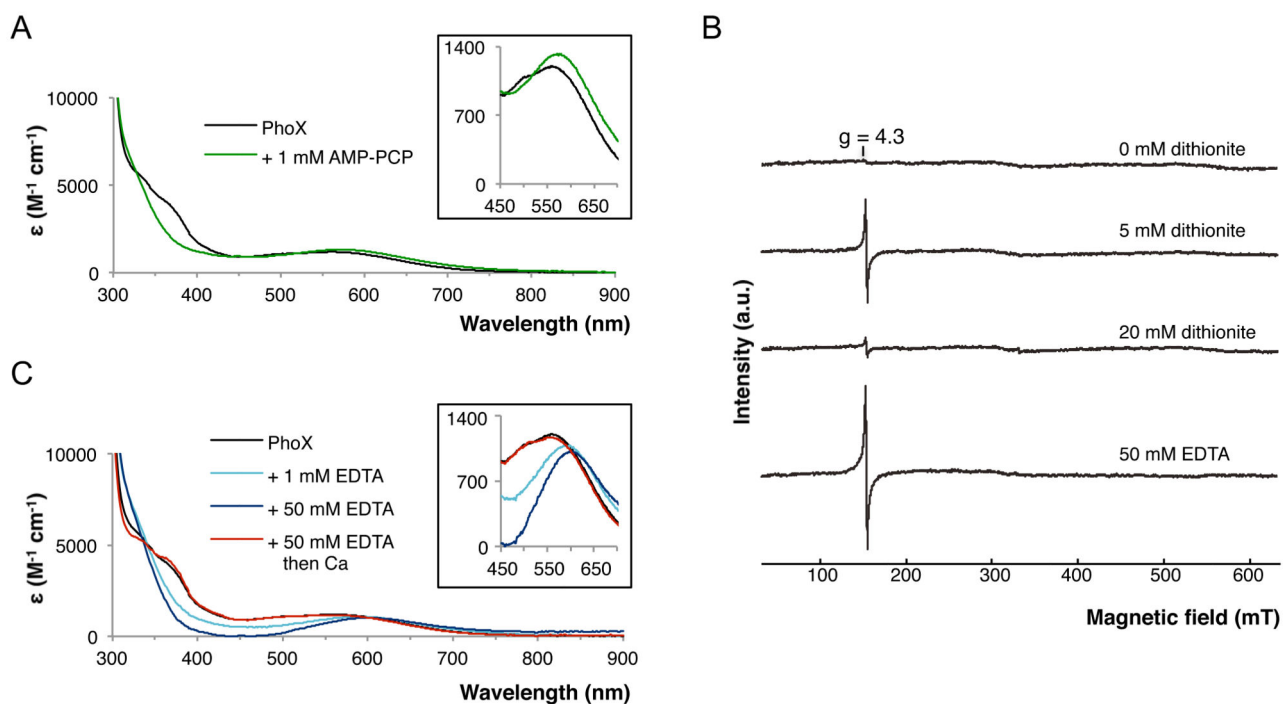


Fig. 1. Spectroscopic analysis of *P. fluorescens* PhoX

(A) Changes in the visible spectrum of PhoX (black line) upon addition of 1 mM AMP-PCP (green line). (B) EPR spectra of PhoX. The sample was progressively reduced with sodium dithionite as indicated. Alternatively the sample was treated with Na_2EDTA . (C) Changes in the visible spectrum of PhoX (black line) upon addition of 1mM (light blue line) or 50mM (dark blue line) Na_2EDTA . The 50mM Na_2EDTA sample was subsequently buffer-exchanged to remove the EDTA and then supplemented with 100mM $CaCl_2$ (red line).

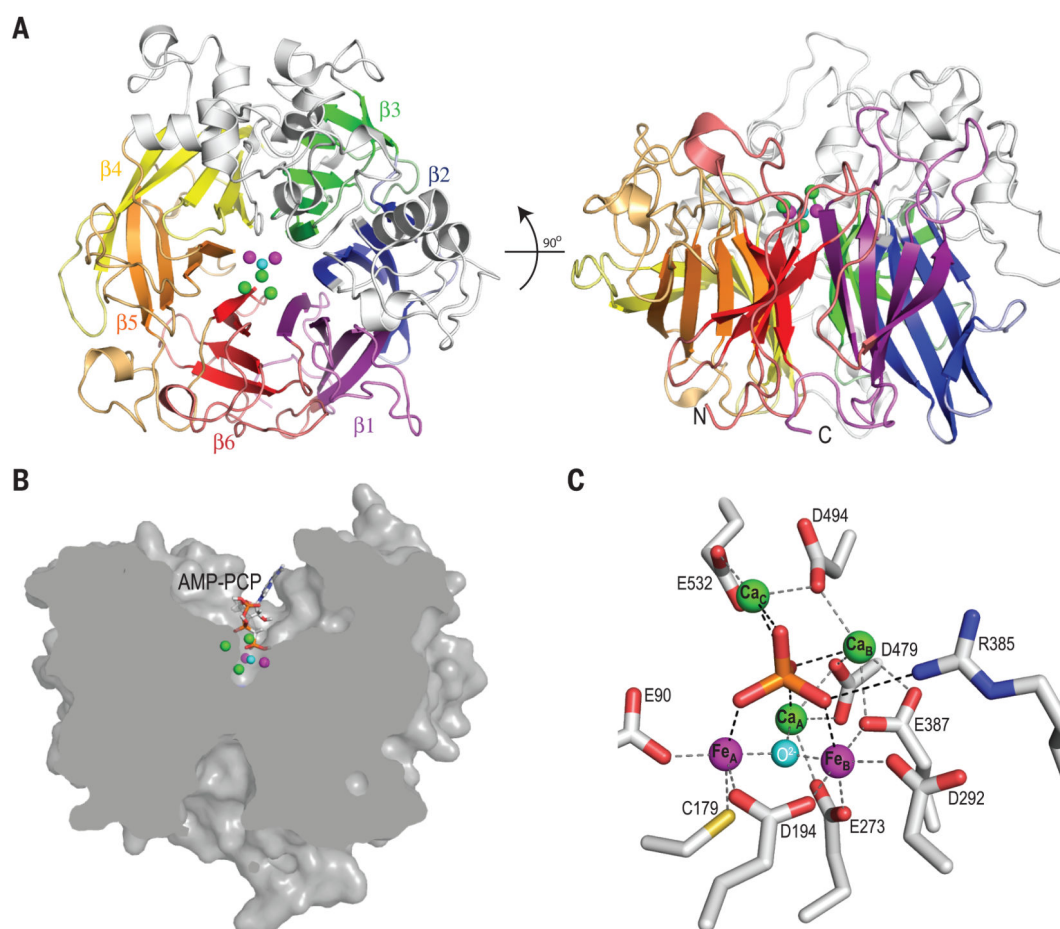


Fig. 2. Structure of *P. fluorescens* PhoX

(A) Cartoon representation of *Pseudomonas fluorescens* PhoX viewed from above the active site (left) or from the side (right). The blades of the β -propeller are shown in different colors and two α -subdomains are colored grey. The active site ions are represented by green (Ca^{2+}), magenta (Fe^{3+}), and cyan (O^{2-}) spheres. (B) Clipped surface representation of PhoX with AMP-PCP bound. (C) The PhoX active site containing bound phosphate. Inter-atomic separations that are within bonding distance are shown between the metals ions and protein side chains (grey dashed lines) and between the phosphate ion and co-ordinating groups (black dashed lines). These distances are tabulated in Table S3.

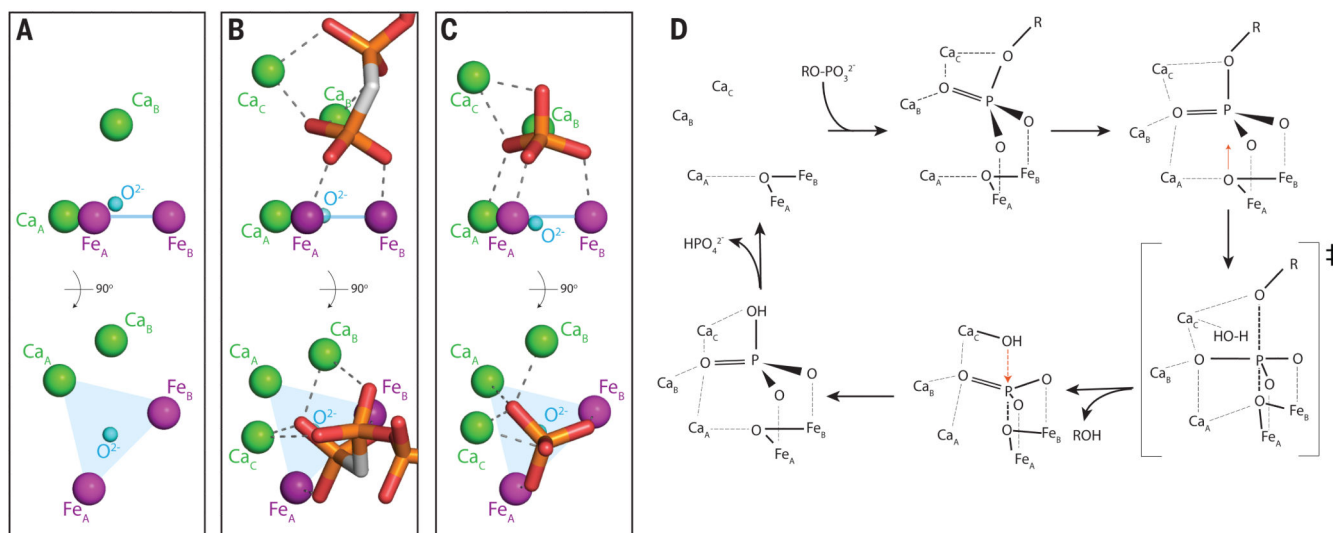


Fig. 3. Ligand binding to the PhoX active site metals and proposed catalytic cycle

(A-C) The active site metal ions and exogenous ligands are viewed from the side (top) and from the direction of substrate access (bottom). Atom representation is as in Fig. 2. Dashed lines indicate ion co-ordination bonds. The plane of the Fe_A-Fe_B-Ca_A ions is shown in blue. Water molecules are omitted for clarity but can be seen in Figs. S4A and S4D. (A) The native enzyme. Ca_C is not present in this structure. (B) The complex with the non-hydrolyzable substrate analogue AMP-PCP. (C) The phosphate complex. (D) Possible model for the mechanism of PhoX. The substrate phosphoryl group initially binds in a tilted orientation (by analogy to the AMP-PCP binding mode) then packs down on to the active site by analogy to the binding mode of phosphate and vanadate. The observed phosphate complex would correspond to the final product complex in this model.